

**Manuscript:**

## **Stiff-sloppy analysis of brain networks to reveal individual differences in task performance**

**Sida Chen<sup>1,2+</sup>, Qianyuan Tang<sup>1,3+</sup>, Taro Toyozumi<sup>3</sup>, Werner Sommer<sup>4,7,8</sup>, Lianchun Yu<sup>5,6\*</sup> and Changsong Zhou<sup>1,2,7\*</sup>**

<sup>1</sup> Department of Physics, Hong Kong Baptist University, Kowloon Tong, Hong Kong

<sup>2</sup> Centre for Nonlinear Studies, Hong Kong Baptist University, Kowloon Tong, Hong Kong

<sup>3</sup> Lab for Neural Computation and Adaptation, RIKEN Center for Brain Science, 2-1 Hirosawa, Wako, Saitama 351-0106, Japan

<sup>4</sup> Institut für Psychologie, Humboldt-Universität zu Berlin, Germany

<sup>5</sup> School of Physical Science and Technology, Lanzhou Center for Theoretical Physics, Lanzhou University, Lanzhou, Gansu 730000, China

<sup>6</sup> Key Laboratory of Theoretical Physics of Gansu Province, and Key Laboratory of Quantum Theory and Applications of MoE, Lanzhou University, Lanzhou, Gansu 730000, China

<sup>7</sup> Life Science Imaging Centre, Hong Kong Baptist University, Kowloon Tong, Hong Kong

<sup>8</sup> Faculty of Education, National University of Malaysia, Kuala Lumpur, Malaysia

## **Abstract**

Understanding how brain networks recruit resources during cognitive tasks is key to explaining individual differences in task performance. Brain network parameters—including activity levels of regions and their connectivity—reflect the integration and segregation of functional subnetworks underlying task processing. However, the complexity and high dimensionality of these parameters pose a significant barrier to identifying functionally relevant individual differences. Here, we introduce stiff-sloppy analysis as a framework for uncovering the stiff parameter combinations that critically influence task-state brain dynamics, exemplified by working memory. Using the pairwise maximum entropy model (PMEM) calibrated to fMRI data and Fisher Information Matrix (FIM) analysis, we reveal that the stiff dimensions of the model parameters capture the most relevant integration and segregation processes of the default mode network and the working memory network. Individual differences along these stiff neural dimensions consistently correlate with working memory performance. Notably, stiff parameters robustly predicted working memory performance, even when the less sensitive (“sloppy”) parameters were excluded. This study establishes stiff-sloppy analysis as a powerful approach to identify cognition-related brain networks, bridging neural dynamics and behavior and offering new avenues for personalized neuroscience including therapeutic innovation.

## Introduction

Individual differences in the brain underpin variability in cognitive and behavioral functions, shaped by genetic, neural, and environmental factors (Baumeister 2007, Bouchard et al. 2003, MacDonald et al. 2009, Thompson et al. 2001). These differences manifest across various scales, including brain anatomy, neural activities, and structural and functional connectivity (Vogel and Machizawa, 2004; Barch et al., 2013; Mueller et al., 2013). Magnetic resonance imaging (MRI) has been instrumental in delineating the neurobiological correlations of individual differences in mental capabilities. However, the complexity and high dimensionality of large-scale brain networks present significant challenges to identifying functionally relevant factors in these individual differences (Faisal et al. 2008). The present study propose to apply a novel framework to identify low-dimensional, functionally relevant individual variance within the high-dimensional variability of brain networks.

A promising solution may be offered by the concept of “sloppiness,” a property observed in many high-dimensional biological systems (Gutenkunst et al. 2007). Sloppiness describes systems where dynamics are insensitive to changes in many “sloppy” dimensions but are highly sensitive to variations in a few “stiff” dimensions. Figure 1 illustrates the core principles of stiff-sloppiness analysis. The parameter space of brain networks can be conceptualized through group-level parameters, representing the “average” system, and individual-level parameters, which deviate from the group and capture individual-specific neural variability. These parameters include activity levels ( $h$ ) of brain region and effective connectivity ( $J$ ) between brain regions, which collectively influence brain network dynamics patterns. Within this framework, the Fisher Information Matrix (FIM) may serve as a tool to differentiate stiff and sloppy dimensions: stiff dimensions correspond to eigenvectors of the FIM with large eigenvalues, indicating high sensitivity of system dynamics to parameter variations, whereas sloppy dimensions are insensitive to parameter changes.

The geometry of sloppy systems underscores how parameter variations impact system dynamics. As shown in Figure 1, variations along stiff dimensions induce significant changes in dynamics, reflecting reconfigurations in brain networks critical for cognitive tasks. Thus, projection of the high-dimensional individual difference in parameters to such stiff directions is supposed to reveal low-dimensional, functionally relevant individual variability underlying individual differences in performance for the given task. Conversely, variations in sloppy dimensions lead to only minimal changes, demonstrating the inherent stability of the system. Therefore, by utilizing these properties, stiff-sloppy analysis isolates functionally relevant variability, linking stiff parameter combinations to cognitive outcomes.

Sloppiness has been investigated in very divers systems, such as in neural networks of animals and in cell cultures (Panas et al. 2015, Ponce-Alvarez et al. 2020, Ponce-Alvarez et al. 2022). In this study, we use stiff-sloppy analysis as a novel framework to link individual differences in human brain parameters to task performance, focusing on the default mode network (DMN) and the working memory network (WMN) with performance in a working memory (WM) task. The DMN and WMN were chosen due to their contrasting roles during working memory tasks: while the WMN, critical for maintaining and manipulating information, is strongly activated (Brookes et al. 2011, Hampson et al. 2010, Raichle 2015) the DMN, typically associated with self-referential and introspective activities, is suppressed. This dynamic interplay makes these networks ideally suited for uncovering the role of sloppiness in brain network dynamics during task processing and exploring functional recruitment beyond the traditional viewpoint of focusing on ROIs of task-related activation. Using the pairwise maximum entropy model

(PMEM) and Fisher Information Matrix (FIM) analysis, we identify stiff dimensions that capture functionally significant reconfigurations of brain networks during WM tasks. By characterizing deviations of individuals from the group mean in activity level and effective connectivity, we demonstrate how stiff dimensions are robustly linked to WM performance.

The sloppiness framework advances our understanding of the relationship between individual brain dynamics and cognitive functioning by isolating low-dimensional, task-relevant variability within high-dimensional neural data. Our findings highlight the potential of sloppiness analysis to provide new insights into the mechanisms of cognitive variability and to inform personalized diagnostic and therapeutic strategies in neuroscience.

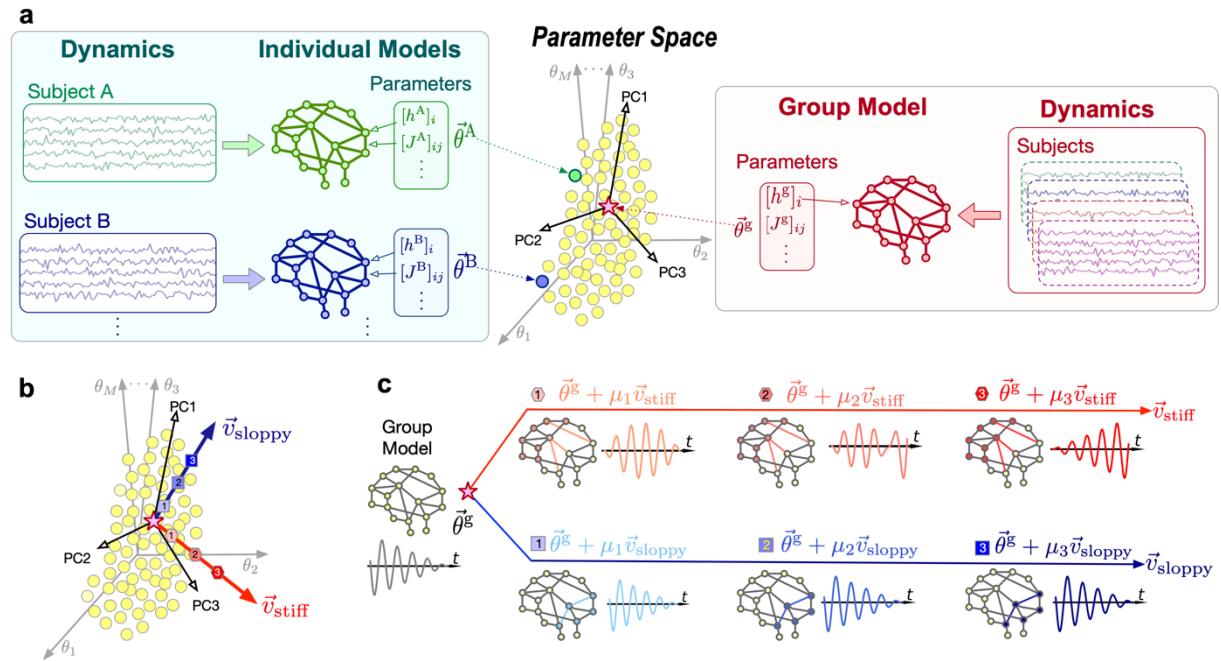


**Figure 1 | Schematic illustrations of parameter space and sloppiness in brain networks.** (a) Illustration of individual model (*left*) and group model (*right*) of brain dynamics. The red pentagram indicates the group parameters  $\vec{\theta}^g$  fitted to the group data. Every small circle refers to the parameters  $\vec{\theta}^q$  fitted to a specific individual  $q$ . Each  $\vec{\theta}$  contains two kinds of parameters  $h$  and  $J$ , corresponding to the activity level within brain regions and effective connectivity between regions, respectively. (b) Geometric properties of stiff and sloppy dimensions. Vectors  $\vec{v}_{stiff}$  and  $\vec{v}_{sloppy}$  refer to the eigenvector of FIM corresponding to larger and smaller eigenvalue, respectively. PC1-PC3 represent the first three components of principal component analysis (PCA) of individual parameters. (c) Effects of variation on system dynamics and stiff-sloppy properties. *Left*: Group model, representing “averaged person” with aggregated dynamics. *Right*: System dynamics under parameter variations along stiff dimensions (top panel, reddish colors) and sloppy dimensions (bottom panel, blueish colors). Equal magnitude parameter variations produce significant dynamic changes only along stiff directions.

## Results

### Large-scale brain networks during task performance are sloppy

We analyzed fMRI signals from 991 participants provided by the HCP database, focusing specifically on the data from the in-scanner WM task. Participants were selected based on their achieving a predefined accuracy threshold during the pairwise maximum entropy model (PMEM) fitting process testing for the emergence of large-scale brain activation patterns (see

Methods for details). We targeted  $N = 21$  (regions of interest) ROIs within the DMN and WMN. PMEM was applied to binarized fMRI signals, estimating two sets of parameters:  $h$ , representing the activity levels of the ROIs, and  $J$ , reflecting the effective connectivity between ROIs. At the group level, data from all participants were concatenated to generate a unified model, while at the individual level, PMEM was applied to each participant, enabling the characterization of individual deviations in brain dynamics as variations in  $h$  and  $J$  relative to the group model (see Fig. 1). This approach highlights individual differences through variability in effective connectivity and activity levels. The PMEM successfully captured functional connectivity patterns in the fMRI data, as the model simulations closely reproduced functional connectivity matrices of the data (see Fig. S1), demonstrating the validity of the approach in modeling brain dynamics during a WM task state for both group and individuals.

To further investigate the system's sensitivity to variations in parameters of effective connectivity and activity levels, naturally induced by individual differences, we performed stiff-sloppy analysis using the FIM of the group model. In the  $M$ -dimensional parameter space ( $M = N + N(N - 1)/2$ ), the FIM characterizes how small perturbations in  $h$  and  $J$  influence brain dynamics. Eigendecomposition of the FIM revealed stiff and sloppy dimensions, with eigenvalues indicating sensitivity along the corresponding eigenvector directions. Stiff dimensions with the largest eigenvalues represent directions in the parameter space where small variations in effective connectivity and activity levels in combination induce significant changes in brain dynamics, whereas sloppy dimensions correspond to directions of parameter change with only minimal impact on brain dynamics. As illustrated in Figure 1, the geometry of sloppiness in parameter space shows that stiff and sloppy directions are distinct. Figure 2 illustrates the workflow of the stiff-sloppy analysis, beginning with normalization and binarization of fMRI signals with a suitable threshold into up and down states, followed by PMEM fitting to estimate effective connectivity and activity levels, computation of the FIM for the group model to capture sensitivity to connectivity variations, and eigendecomposition of the FIM to identify stiff and sloppy dimensions (see Methods).

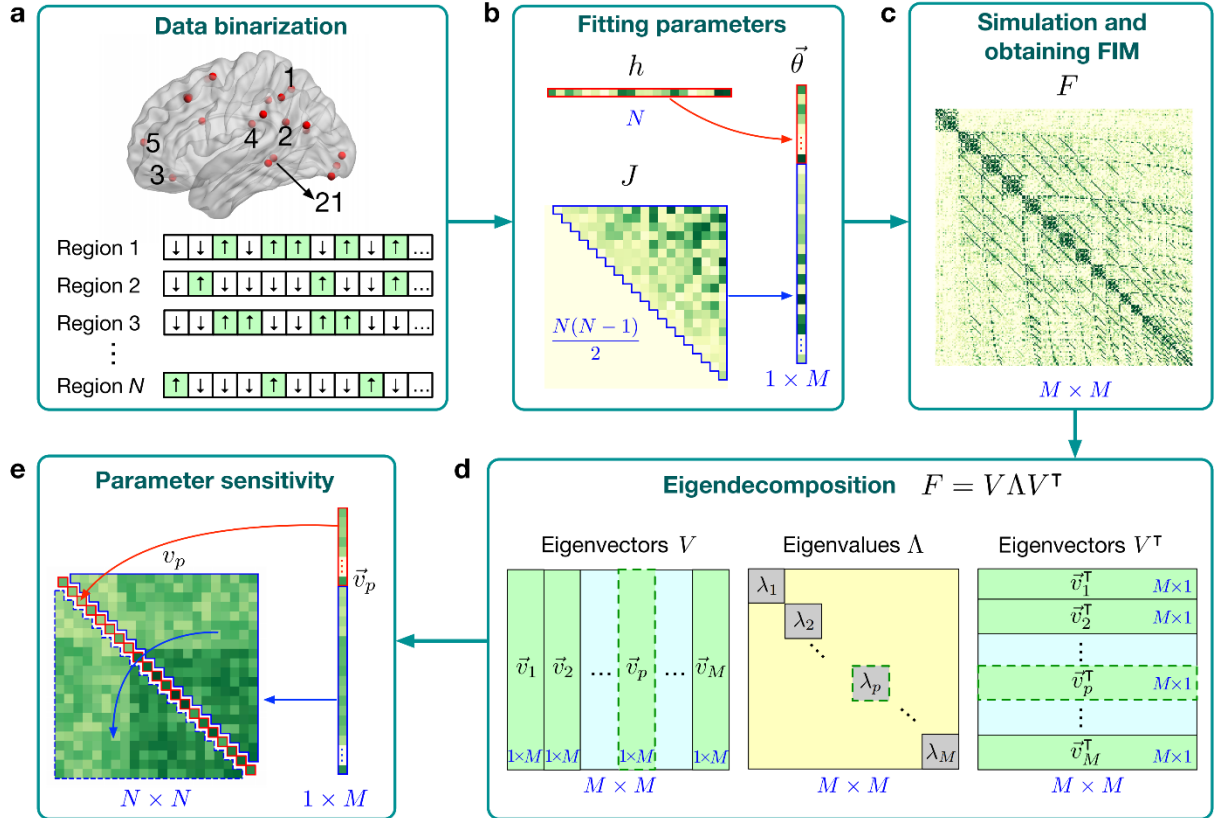


**Figure 2 | Workflow of stiff-sloppy analysis of brain networks** (a) Normalizing and binarizing the fMRI signals over time with a suitable threshold into up and down states (arrows). Red dots denote the centers of regions of interest (ROI). (b) Fitting the parameters of PMEM. In parameter space, each model can be represented by an  $M$ -dimensional vector of parameters  $\vec{\theta}$  where  $M$  is the number of parameters. Each parameter vector contains the  $N$ -dimensional external field  $h$  and the  $N(N - 1)/2$ -dimensional effective connectivity  $J$ . (c) Calculation of FIM. (d) The eigendecomposition of FIM yields eigenvalues and eigenvectors. (e) The elements of eigenvector  $\vec{v}_p$  have the one-to-one correspondence to model parameters  $\vec{\theta} = (h, J)$ . For the working memory task state analyzed in this study,  $N=21$ ,  $M=231$ .

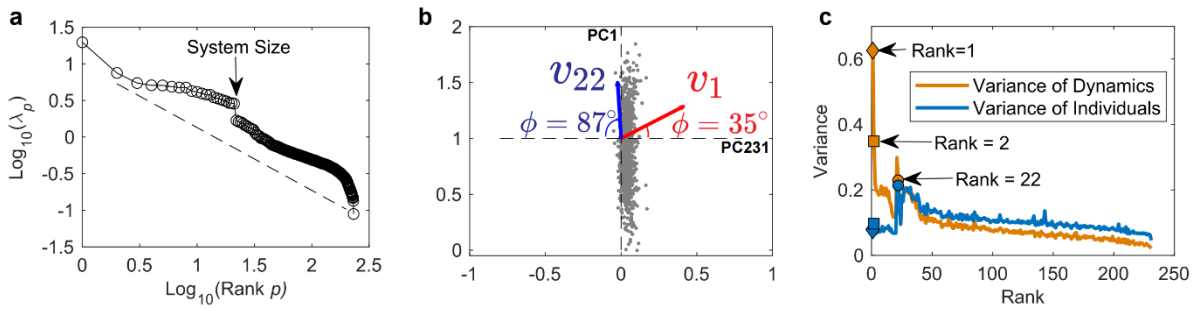


**Figure 3 | Large-scale brain networks during task state are sloppy.** (a) The rank-ordering distribution of FIM eigenvalues for the group model. The black dashed line represents eye-guiding power-law trend (scaling coefficient of  $-0.86$ ). (b) Geometric relationship between PCA components and eigenvectors of FIM. Each gray dot is an individual projection of parameters on the subspace of PC1 and PC231. The surface of eigenvectors ( $v_1$  and  $v_{22}$ ) and the surface of PCs (PC1 and PC231) are not coplanar. (c) Variance of parameters across individuals along FIM eigenvectors and its effect on dynamics variation across individuals. Eigenvectors of FIM are ranked according to the eigenvalues.

Our analysis demonstrates that large-scale brain networks during the WM task state exhibit sloppiness properties, as evidenced by the broad, power-law like distribution of eigenvalues in the FIM and their associated eigenvectors. Figure 3a highlights the rank-ordered distribution of eigenvalues derived from the FIM for the group model, which was constructed using data from all participants. The eigenvalues exhibit a power-law-like distribution, with the first 21 eigenvalues (corresponding to the number of ROIs in the system = system size) showing negative but close-to-zero exponents, whereas the remaining eigenvalues display a more strongly negative exponent. This pattern suggests the presence of stiff dimensions within the modeled brain system with significant impact on brain dynamics.

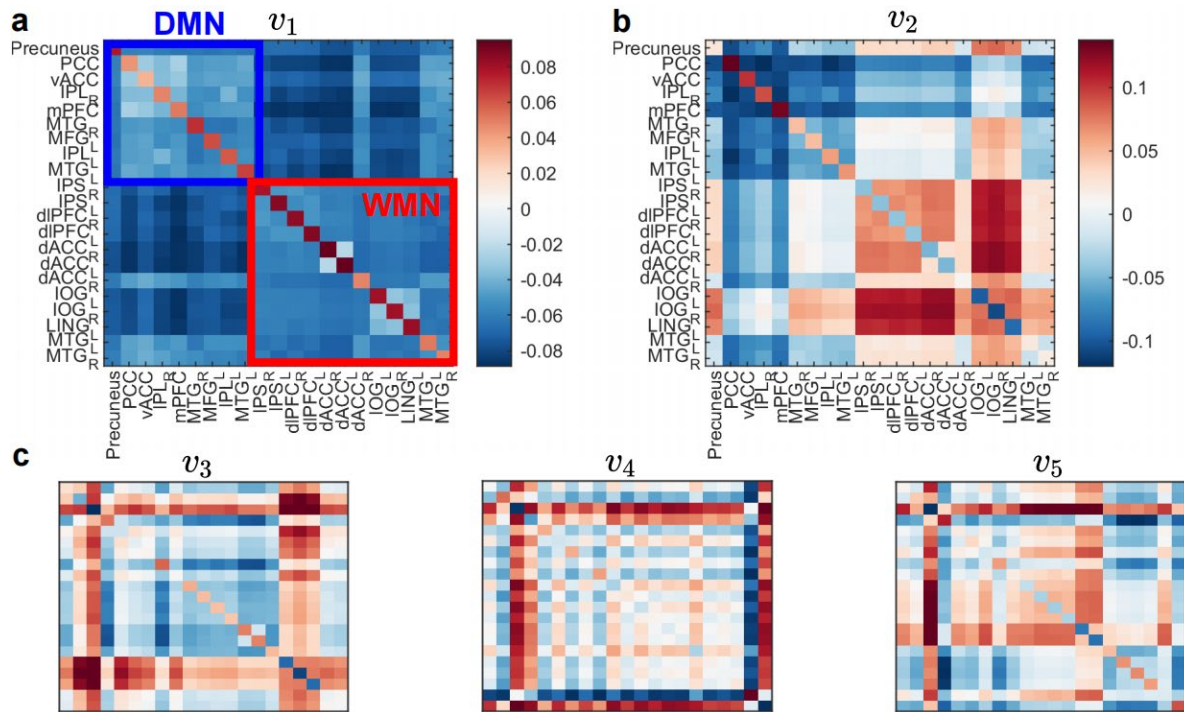
The effects of parameters on brain dynamics arise from two factors: variations in parameters across individuals and the sensitivity of brain dynamics to those variations. To understand this interaction, we analyzed the relationship between two elements: (1) the principal components (PCs) that describe how parameters vary across individuals, and (2) the eigenvectors of the Fisher Information Matrix (FIM), which represents how sensitive brain dynamics are to change in these parameters. PCA identifies the main directions of parameter variation across individuals, with the first principal component corresponding to the direction of the greatest variance. Following the sloppiness property, a larger parameter variation in a sloppy direction may not have as strong impact on dynamics variation as induced by even a smaller parameter variation in a stiff direction. To maintain the stability of the system, actual individual differences of parameters in the stiff dimensions might be smaller than that in the sloppy directions. To examine this, we calculated the pairwise cosine similarity between the 231 PCA components (derived across parameters of individual models) and the 231 eigenvectors of the FIM of the group model. The pairwise similarity matrix (Fig. S2) reveals distinct patterns: the first 21 eigenvectors (stiff dimensions) align closely with PCA components with smaller loadings, forming a back-diagonal structure. In contrast, the other eigenvectors roughly align with PCA components of the same rank, creating a diagonal structure. This is further illustrated by the angles between PC231 and specific eigenvectors: the angle between PC231 and  $\vec{v}_1$  is  $35^\circ$ , while the angle between PC231 and a sloppy direction  $\vec{v}_{22}$  is  $87^\circ$  (Figure 3b) (the angle between PC1 and  $\vec{v}_1$  is  $84^\circ$ , while the angle between PC1 and a sloppy direction  $\vec{v}_{22}$  is  $72^\circ$  (Figure S3)). These results demonstrated that individual difference has small variation along stiff directions, while strong parameters variation happen more easily along the sloppy directions.

Figure 3c illustrates the variance of parameters across individuals projected onto FIM eigenvectors and their effects on system dynamics. Parameter variance peaks at  $\vec{v}_{22}$ , while the first 21 eigenvectors (stiff dimensions) show relatively low variance, comparable to that of sloppy dimensions (specifically, eigenvectors between  $v_{21}$  and  $v_{211}$ ). The effect of parameter variation along an eigenvector  $\vec{v}_p$  on dynamics can be quantified by projection of the empirical functional connectivity of individuals on  $\vec{v}_p$ , denoted as

$$\text{Var}_{\text{Dynamics}}(p) = \text{Var}(FC_{\text{empirical}}^q \cdot \vec{v}_p),$$

where  $q$  denotes the  $q$ -th participant, and  $\text{Var}$  denotes the variance over all participants. As seen in Figure 3c, despite the large parameter variance of individuals along  $\vec{v}_{22}$ , its effect on dynamics is lower than that of  $\vec{v}_1$  and  $\vec{v}_2$ , which show the smallest inter-individual variance of parameters but have the largest effects on dynamics (FC). These results clearly demonstrate the stiff-sloppy properties of the system. This finding also challenges the conventional assumption that dimensions with the largest inter-individual variability are functionally most relevant. Instead, our results show that stiff dimensions, characterized by their large impact on dynamics, exhibit relatively low inter-individual variance, underscoring their critical functional importance.

Figure 4 illustrates the structure of the eigenvectors from the FIM by mapping them back to matrix form, where each entry corresponds to regional activity level  $h_i$  (diagonal entries) or effective connectivity  $J_{ij}$  between ROIs  $i$  and  $j$  (off-diagonal entries). The heatmap visualization provides insights into the sensitivity of each parameter along a given eigenvector to induce changes in brain network dynamics. Figure 4a–4c highlight how different eigenvectors emphasize distinct aspects of network dynamics. Along the  $\vec{v}_1$  direction, which represents the stiffest dimension with the largest eigenvalue, individual differences are predominantly reflected in the global segregation between the DMN and WMN, characterized by weaker effective connectivity between these networks. Conversely, the  $\vec{v}_2$  direction reflects more localized functional integration; along  $\vec{v}_2$  individual differences are associated with strengthened effective connectivity within the WMN. Higher-order eigenvectors, such as  $\vec{v}_3$  and beyond, exhibit increasingly complex and localized patterns of sensitivity. However, to simplify the analysis, we focus on the first and second eigenvector of the FIM, as they capture the most critical aspects of individual variability in brain dynamics (Figure 3c).



**Figure 4 | Eigenvectors of FIM (a-c)** Eigenvectors of the FIM for the group model. Blue and red rectangles in (a) highlight the parameters associated with the default mode network (DMN) and the working memory network (WMN), respectively. The heatmap represents the weights of the entries, indicating the sensitivity of the parameters along a given eigenvector to induce changes in brain network dynamics. Warm colors (e.g., red) indicate positive sensitivities, while cold colors (e.g., blue) indicate negative sensitivities in the relationship between parameter variance and dynamics.

### Individual differences of parameters along the stiff dimensions are associated with the dynamic segregation and integration of brain functional networks.

Next we demonstrate that individual differences in effective connectivity  $J$  and activity levels  $h$  along stiff directions are associated with the dynamic integration and segregation of brain functional networks during the WM task state. To quantify these differences, we defined the variation of parameters across participants with respect to group values along the eigenvectors

of the FIM as  $\eta_p^q = (\overline{\theta}_q - \overline{\theta}_g) \cdot \overline{v}_p^g$ , where  $q$  represents individual subjects,  $g$  represents the group, and  $p$  denotes the rank of the eigenvector. This value,  $\eta_p^q$ , reflects how individual configurations deviate from the group along specific eigenvector directions. FC of each subject was calculated as the average FC across all connections within the DMN, within the WMN, or between the two subnetworks (denoted as BTN). Here, FC between two ROIs was calculated as Pearson's correlation of the fMRI signals of the ROIs. A higher average FC indicates greater integration, while a lower average FC reflects increased segregation.

Figure 5 illustrates the relationship between  $\eta_1$  and  $\eta_2$  and the integration or segregation of brain networks during the task state. Panels 5a–5c show scatter plots of the average FC within the DMN, within the WMN, and between the DMN and WMN as a function of  $\eta_1$ . Panels 5d–5f depict the same relationships for  $\eta_2$ . As  $\eta_1$  increases, the average FC within the DMN shows a weak but significant negative correlation (Fig. 5a), reflecting increased segregation within the DMN. Similarly, the average FC within the WMN decreases slightly with increasing  $\eta_1$  (Fig. 5b), indicating reduced integration within the WMN. In contrast, the average FC between the DMN and WMN (BTN) exhibits a strong negative correlation with  $\eta_1$  ( $r = -0.7935$ ; Fig. 5c), suggesting that larger  $\eta_1$  values correspond to greater segregation between these two networks. For  $\eta_2$ , a different pattern emerges. The average FC within the WMN is strongly positively correlated with  $\eta_2$  ( $r = 0.6006$ ; Fig. 5e), reflecting enhanced integration within the WMN as  $\eta_2$  increases. The average FC within the DMN, however, exhibits a weak but significant negative correlation with  $\eta_2$  (Fig. 5d), indicating a slight segregation within the DMN along this direction. Notably, there is no significant correlation between  $\eta_2$  and the average FC between the DMN and WMN (BTN; Fig. 5f), suggesting that  $\eta_2$  primarily influences integration within individual subnetworks rather than integrating DMN and WMN together.

Together, these findings highlight the distinct roles of  $\eta_1$  and  $\eta_2$  in shaping the integration and segregation strategies of brain networks during the WM task state. Specifically,  $\eta_1$  is associated with increased segregation within both DMN and WMN and reduced integration between the two networks, while  $\eta_2$  corresponds to enhanced integration within the WMN but slight segregation within the DMN. These results emphasize how stiff directions in parameter space reflect critical aspects of individual differences in brain functional organization during task performance.

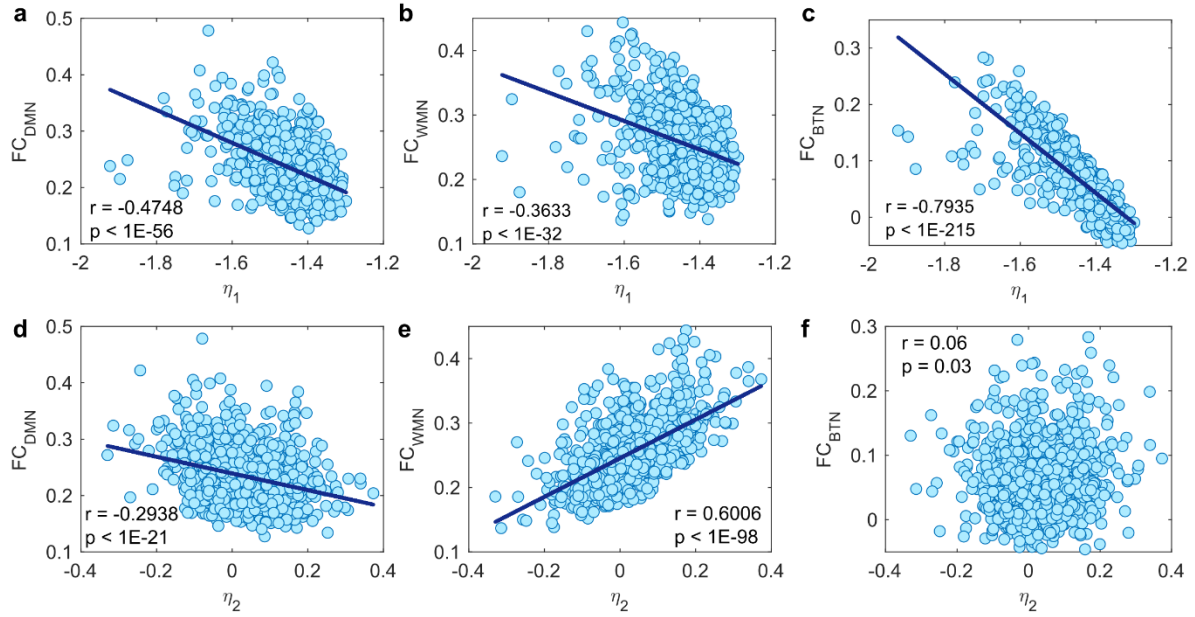


**Figure 5 | Individual differences of parameters along the stiff dimensions indicate the dynamic segregation and integration of functional brain networks.** (a-c) Scatter plots of the change in FC versus  $\eta_1$  across individuals. (d-f) Scatter plots of the change in FC versus  $\eta_2$  across individuals. The subscripts "DMN", "WMN" and "BTN", respectively denote that we exclusively consider the connections within DMN, within WMN and the connections between DMN and WMN (i.e., BTN). The blue solid lines show the least-squares fitting with the Pearson's correlation coefficient  $r$  and the  $p$ -value in the corresponding panel.

### Task performance is robustly predicted by a few sensitive parameters.

Next, we show that stiff directions provide robust predictions of subjects' WM task performance, demonstrating their generalizability across datasets and the validity of stiff-sloppy analysis in revealing brain network recruitment in cognitive process. To evaluate this, we divided the full dataset into a training set and nine test sets in a 10-folder scheme. The group model was fitted using the training set to derive the stiff directions, which were then used to project individual parameter variations from each test set, yielding predicted  $\eta_p$ . Pearson's correlation was calculated between these predictions and participants' WM performance accuracy. As shown in Figure S4, only  $\eta_1$  and  $\eta_2$  show significant prediction of WM performance, while other dimensions do not show strong predictability. As demonstrated in earlier sections,  $\eta_1$  and  $\eta_2$  correspond to distinct integration and segregation strategies (Fig. 5). To balance these global and localized processes, we computed a combined parameter,  $\eta_{tot} = \alpha\eta_1 + (1 - \alpha)\eta_2$ , and adjusted  $\alpha$  from 0 to 1 to find the optimal combination ratio.

As shown in Figure 6a, the combination  $\eta_{tot}$  achieved the highest predictability of WM accuracy at  $\alpha = 0.48$ , determined via 10-fold cross-validation. This result suggests that combining global segregation ( $\eta_1$ ) and localized integration ( $\eta_2$ ) in the proper proportion enhances predictive power, highlighting the significance of balancing these two functional recruitment strategies. Such an optimal ratio can also be derived from theoretical analysis based on the eigenvalues  $\lambda_1, \lambda_2$  representing the sensitivity of parameter variation along  $\vec{v}_1, \vec{v}_2$  (see Methods) at  $\alpha = 0.61$  (red dot in Fig. 6a), coinciding with the empirical correlation peak within

the error range. Figure 6b further illustrates this relationship, with a scatter plot showing the strongest correlation between  $\eta_{tot}$  (at  $\alpha = 0.48$ ) and subjects' task accuracy.

To test the robustness of predictions made using  $\eta_{tot}$ , we examined the sensitivity of parameters along the combined stiff direction  $\overrightarrow{v_{tot}} = \alpha \overrightarrow{v_1} + (1 - \alpha) \overrightarrow{v_2}$  at the optimal  $\alpha = 0.48$ . The parameters were ranked by their sensitivity, defined as the absolute value of the corresponding elements in the combined vector  $\overrightarrow{v_{tot}}$ . Parameters with lower sensitivity (sloppy parameters) were progressively removed (set to zero value) to obtain the sparsified  $\overrightarrow{v_{tot}^s}$  and  $\eta_{tot}$  is recalculated by projecting individual parameters onto  $\overrightarrow{v_{tot}^s}$ ; then we evaluated their impact on predictability. As shown in Figure 6c, removing the least sensitive 20% of parameters improved predictability, reaching a peak correlation. Even after discarding up to 80% of the least sensitive parameters, the correlation between  $\eta_{tot}$  and working memory accuracy remained significant, demonstrating the robustness of stiff directions and sensitive parameters in predicting WM performance.

Based on the sparsified  $\overrightarrow{v_{tot}^s}$  at 80%, we assessed the functional roles of specific ROIs by averaging the sensitivity of their connections. Figure 6d identifies the top four ROIs with the highest positive sensitivity (located in dlPFC, IPS, IOG, LING) and the top four with the highest negative sensitivity (located in mPFC, IPL, PCC, MTG). Notably, all connections between high-positive-sensitivity ROIs and high-negative-sensitivity ROIs exhibited negative values. Positive sensitivity indicates that more positive effective connectivity enhances WM performance, whereas negative sensitivity indicates that more negative effective connectivity is associated with better performance. ROIs with the highest positive sensitivity (located in dlPFC, IPS, IOG, and LING) are ROIs of the WMN primarily involved in the integration of WM-related processes (Moser et al. 2018). Connections between these ROIs showed positive sensitivity, suggesting that stronger functional integration within these areas supports improved WM performance. This highlights their central role in efficient recruitment of resources for task execution. On the other hand, ROIs with the highest negative sensitivity (located in mPFC, IPL, PCC, and MTG) are associated with the DMN and typically exhibit segregation during WM task performance. Negative sensitivity in these ROIs suggests that reducing their effective connectivity enhances task accuracy. This aligns with prior findings that suppressing DMN activity facilitates cognitive tasks requiring attention and memory resources (Anticevic et al. 2012).

### **Coordinated interplay between multiple networks in WM task processing: Comparisons with Alternatives**

Besides our proposed stiff-sloppy analysis method, we also evaluated the Connectome-based Prediction method (CPM) (Shen et al. 2017) for identifying key brain connections. As shown in Figure S5, both methods employ 10-fold cross-validation but differ fundamentally in approach. While CPM can achieve good prediction by selecting significant functional connections from the training set, its selected features vary substantially across iterations, indicating low consistency and low robustness. In contrast, sloppiness analysis identifies stiff directions that not only provide stronger predictive power for WM task accuracy but also maintain highly consistent features independent of sampling variations. This comparison demonstrates the superior robustness and reliability of the stiff-sloppy analysis in identifying brain-behavior relationships.

To investigate the role of individual functional networks in explaining WM performance, we applied the stiff-sloppy analysis to models fitted exclusively on either the DMN or the WMN. The results reveal that isolating these networks reduces correlations of stiff directions with WM task performance, highlighting the critical role of their interaction in supporting cognitive performance. In the DMN-only model,  $\eta_1$  showed a significant but weak correlation with working memory task accuracy. Conversely, in the WMN-only model,  $\eta_2$ , associated with local integration, exhibited a similarly significant but weak correlation with task accuracy (Figure S4). Interestingly, the eigenvector  $v_2$  from the WMN-only model resembled the WMN-related portion of the eigenvector structure in the full model (incorporating both DMN and WMN) (Figure 4b). This similarity underscores the role of localized integration within the WMN in supporting WM processes.

The reduced correlations observed in these isolated models compared to the full model highlight the necessity of accounting for dynamic interactions between the DMN and WMN in explaining WM performance. It is not sufficient to examine only the WM network localized during WM processing. These findings emphasize that cognitive performance relies on the coordinated interplay of multiple networks rather than the properties of individual networks in isolation.

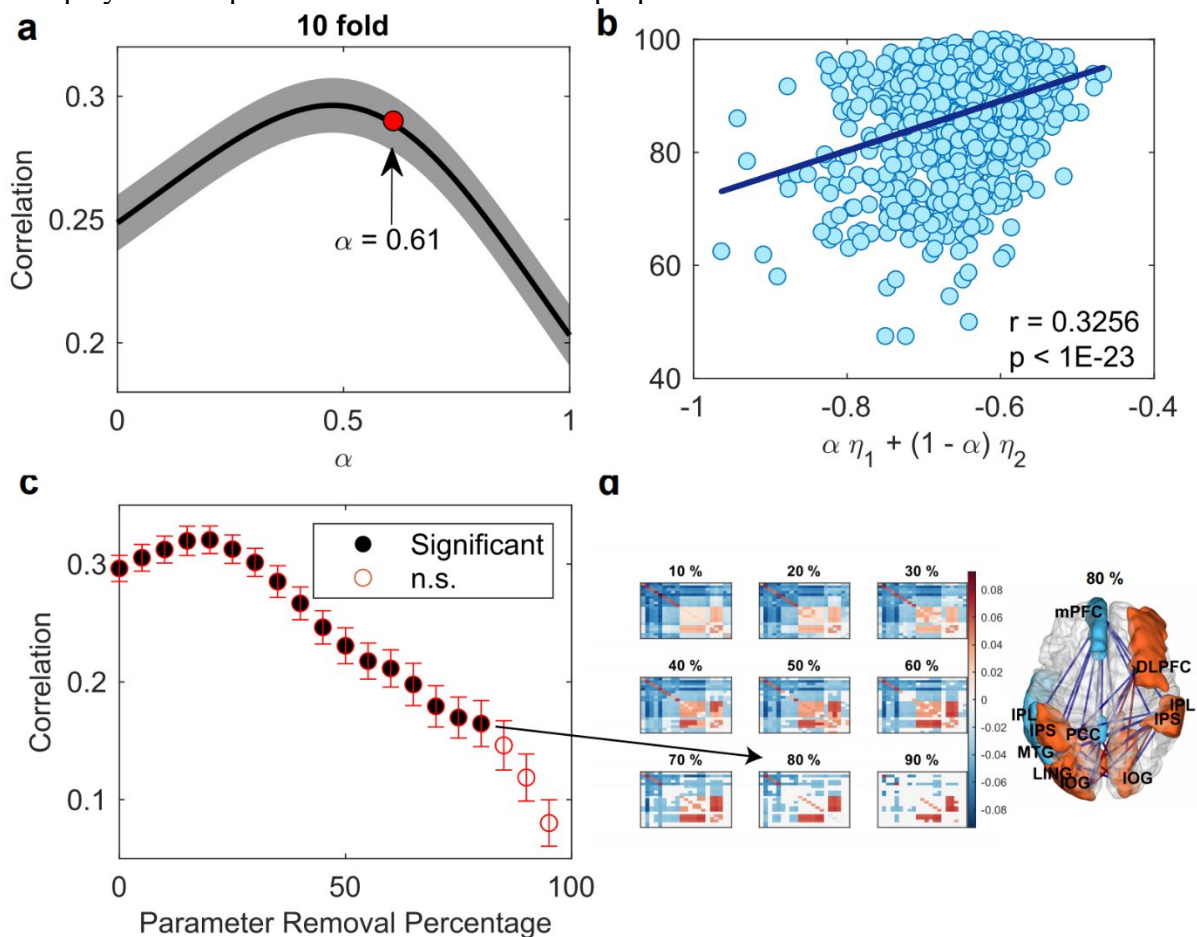


**Figure 6 | Individual differences in parameters along the stiff dimensions are associated with task performance.** (a) Searching for the optimal combination ratio  $\alpha$  via 10-fold cross validation. The shaded area shows the standard deviation of 10 realizations of cross validation. In the test sets, the correlation is calculated as Pearson's correlation between  $\eta_{\text{tot}} = \alpha\eta_1 + (1 - \alpha)\eta_2$  and participants' WM accuracy. Red dot shows the theoretical optimal  $\alpha$  and corresponding correlation. (b) Scatter plot of the accuracies of individuals in the WM task versus the optimal combination  $\eta_{\text{tot}}$  ( $\alpha = 0.48$ ). The blue line shows the least-squares fit with Pearson's correlation coefficients  $r$  and the  $p$ -value. (c) Robustness of the stiff parameters. Progressively discarding the least sensitive parameters leaves

Pearson's correlation between  $\eta_{tot}$  at  $\alpha = 0.48$  and WM accuracy relatively stable and significant ( $p$ -values  $< 0.0001$ ) up to a loss of 80% of the insensitive parameters. (d) *Left*: Sparsification of stiff dimension components ( $\overrightarrow{v_{tot}^S}$ ) by progressively removing 10%, 20% to 90% of the least sensitive parameters. *Right*: ROIs with the highest positive sensitivity and the ROIs with the highest negative sensitivity after removing 80% of the least sensitive connections. Blue lines represent connections with negative values in the sparsified  $\overrightarrow{v_{tot}^S}$  (more negative values in individuals with higher WM accuracy), while red connections represent connections with positive values in  $\overrightarrow{v_{tot}^S}$  (more positive values in individuals with better WM accuracy). The blue and red ROIs show negative and positive mean sensitivity, respectively, after averaging the sensitivity of connections based on  $\overrightarrow{v_{tot}^S}$ . (DLPFC = dorsolateral prefrontal cortex; mPFC = medial prefrontal cortex; IPL = inferior parietal lobule; IPS: intraparietal sulcus; IOG = inferior occipital gyrus; LING = lingual gyrus; MTG = middle temporal gyrus; PCC = posterior cingulate cortex)

## Discussion

Our study introduces stiff-sloppy analysis as a novel framework for understanding individual differences in brain network dynamics during cognitive tasks. While previous approaches have focused on analyzing network properties through graph theoretical measures (Bullmore et al. 2009) or statistical techniques (Smith et al. 2015), these methods often struggle to link dynamics, brain networks, and individual differences in behavior. Brain network parameters—including activity levels of regions and their connectivity—govern the integration and segregation of functional subnetworks serving for task processing, but their complexity and high dimensionality have remained a persistent challenge (Medaglia et al. 2015). Our approach reveals that while individual brains may vary considerably along many dimensions, only variations in a few specific "stiff" dimensions are significantly associated with cognitive performance. These stiff dimensions, much like essential control parameters in complex systems, have outsized effects on brain function despite showing relatively low variance across individuals—a property that manifests stiff-sloppy properties of task states of the brain. By identifying these key dimensions, we provide a novel bridge between neural organization and behavior that aligns with functional network specializations.

### Stiff Dimensions and Individual differences

A central finding of our work is that stiff dimensions—parameters with outsized effects on system dynamics—exhibit low inter-individual variability (Figure 3b, 3c). This result challenges the conventional assumption that the functionally most relevant parameters are those with the largest variability across individuals (Finn et al. 2015, Gratton et al. 2018). However, our findings align with theoretical work suggesting that certain network properties must be tightly regulated for optimal function (Honey et al. 2010), and extends this concept to identifying specific dimensions critical for cognitive performance in a WM task. This insight helps resolve a key dilemma in brain modeling. While brain activity patterns vary substantially across individuals, successful task performance consistently depends on specific configurations of these stiff dimensions. By identifying these key parameters that link brain organization to behavior, the stiff-sloppy analysis provides a more focused framework for understanding individual differences that are hidden behind apparent variations. Rather than attempting to capture all variations in high-dimensional brain data, we can now prioritize a small set of relatively invariant parameters that genuinely matter for cognitive function and their individual manifestation.

## Dynamic Network Reconfiguration Through Stiff Dimensions

For the first time, we show that stiff dimensions are critical for understanding how the brain dynamically recruits resources to meet cognitive demands. While previous studies, such as (Cole et al. 2013) and (Shine et al. 2016), have demonstrated task-dependent reconfigurations of brain networks, their approaches relied on distinct methodologies. Cole et al. used functional connectivity analyses to identify task-general and task-specific network reconfigurations across diverse cognitive tasks, emphasizing the dynamic flexibility of the brain's core network. Shine et al. employed graph-theoretic metrics, such as modularity and global efficiency, to capture changes in network topology during cognitive control tasks, highlighting shifts in integration and segregation across brain regions. In contrast, our approach uniquely identifies the specific network parameters driving these changes. The observed DMN-WMN antagonism aligns with prior work (Anticevic et al. 2012, Fox et al. 2005), but provides a novel mechanistic framework for understanding how this relationship impacts cognitive performance. Specifically, the projection along the stiffest dimension ( $\eta_1$ ) captures global segregation between the DMN and WMN, and the projection along the second stiffest dimension ( $\eta_2$ ) reflects local integration within the WMN. Stronger DMN-WMN segregation correlates with better task performance (Figure 5c & Figure 6a), suggesting effective suppression of self-referential thought helping to prioritize task-relevant cognition. Similarly, enhanced integration within the WMN ( $\eta_2$ ) supports better WM performance (Fig. 5e & Fig. 6a).

Our findings provide compelling evidence that stiff dimensions represent fundamental principles of brain organization, as they show remarkably consistent effects on network reorganization during cognitive tasks while maintaining stability (relatively little variance) across individuals. This network-level perspective is crucial: when DMN and WMN were analyzed separately, using sloppiness analysis, predictability of task performance decreased significantly (Fig. S4), confirming that cognitive function emerges from coordinated interactions between networks rather than from isolated brain systems. Here we only considered DMN in addition to the localized WMN in WM tasks. It is plausible to speculate that the predictability could be improved if other parts of the brain than just DMN and WMN are taken into account, and the same could be extended to other tasks. When extending to larger networks, it is likely that more stiff dimensions would need to be taken in consideration to form combined a low-dimensional direction to give optimal prediction of performance outcomes. This finding and its further validation in future work with whole-brain model and more tasks are expected to have far-reaching implications for cognitive enhancement and neuromodulation. For example, to effectively enhance working memory, it would not be sufficient just to focus on WMN (or typically just one region, e.g. DLPFC). In contrast, it is essential to make perturbation in the combined stiff direction, for example, to enhance the connectivity within WMN and simultaneously reduce the connectivity with DMN (Figure 6).

## Robustness and Predictive Power

The stiff-sloppy analysis demonstrates robust predictive capabilities, even with limited data. While recent machine learning approaches have shown promise in predicting individual differences (Rosenberg et al. 2016, Shen et al. 2017), our method achieves comparable or better performance while providing mechanistic insights into the underlying network organization. Using a 10-fold validation approach, we showed that task performance for a large test set of around 900 subjects could be reliably predicted using models trained on only 90 subjects (Figure S3a). Stiff-sloppy analysis consistently identified task-relevant, dynamic networks with greater reliability than the CPM method which struggled to generate stable functional networks underlying the cognitive process. Our results further demonstrated that removing redundant parameters—those associated with sloppy dimensions—improves model predictability (Figure

6c). By isolating the minimal set of parameters necessary to explain behavior, this approach enables the development of parsimonious models with enhanced explanatory power, making them more suitable for applications in neuroscience and clinical diagnostics.

In the current work, we demonstrated the stiff-sloppy analysis with working memory tasks, focusing on relatively small subnetwork of WMN and DMN. Future work will explore the expansion to whole-brain networks, other tasks and latent abilities such as fluid intelligence.

### **Implications for Brain Organization and Clinical Applications**

The implications of our findings extend beyond working memory tasks, offering insights into general principles of brain organization subserving human abilities. Stiff dimensions may reflect the core functional rules that enable efficient recruitment and reconfiguration of networks under task processing, while sloppy dimensions accommodate variability without disrupting essential functions. The implications extend beyond working memory to broader questions of brain organization and function. Previous work has shown that brain networks can flexibly reconfigure for different cognitive demands (Cole et al. 2013, Shine et al. 2016, Wang et al. 2021), but the mechanisms enabling this flexibility while maintaining stability remain unclear. Our identification of stiff and sloppy dimensions offers a potential solution: stiff dimensions may provide the stable scaffolding necessary for consistent performance, while sloppy dimensions create the flexibility needed for adapting to varying cognitive demands. Future research examining these dimensions across multiple cognitive tasks could reveal how the brain achieves this balance between stability and adaptability during task switching and multi-task processing.

This approach also has promising clinical applications, particularly for understanding and treating psychiatric conditions. Previous studies have characterized psychiatric disorders using static network metrics - such as graph theoretical measures of modularity, clustering coefficients, and path lengths (Baker et al. 2014), or resting-state functional connectivity patterns (Drysdale et al. 2017). The identification of stiff dimensions could help refine strategies for interventions like TMS, moving beyond single-region approaches (Fox et al. 2012) to network-based targeting. For example, effective neuromodulation treatment of cognitive decline in working memory may target a set of most sensitive brain regions in WMN (not just one region DLPFC), and importantly, goes beyond the traditional localization of such task-evoked regions to simultaneously suppress sensitive regions in DMN (Figure 6d). The stability of stiff-sloppy analysis with respect to relatively small sample size underscores its utility in clinical research, particularly when sample sizes are limited.

Looking forward, our framework can be extended to other cognitive domains and neurological conditions while integrating multiple data types such as EEG, MEG, and fMRI. This integration across temporal and spatial scales could uncover universal principles of brain dynamics, particularly how stiff-sloppy organization manifests in different contexts and populations.

## **Methods**

### **Experimental techniques**

#### **fMRI data acquisition and preprocessing**

We utilized data from the HCP database (<http://www.humanconnectome.org>) (Barch et al. 2013) including 991 healthy participants selected based on the following criteria: (1) the availability of Working Memory (WM) Task Overall Accuracy records, and (2) convergence to a fitting accuracy of 0.99 in a pairwise maximum entropy model, which will be explained below. Neuroimaging data were

acquired using a Siemens Skyra 3T scanner and preprocessed in accordance with standard HCP protocols. The WM task implemented in the HCP features a block design with alternating experimental (2-back) and sensorimotor control (0-back) conditions. Each block began with a 2.5-s written cue indicating the condition (2-back or 0-back) and the designated target stimulus for the control condition. Stimuli from four categories (faces, places, tools, and body parts) were presented in separate blocks. Each stimulus appeared for 2 s, followed by a 500-ms inter-stimulus interval. During 2-back trials, participants responded by pressing a button when the current stimulus matched the one presented two trials earlier, while in 0-back trials, they responded to a pre-specified target stimulus. To analyze HCP task-based fMRI data, we utilized the FEAT analysis tool after applying the HCP minimal preprocessing pipelines (Woolrich et al. 2009). For scan-level analyses, we based our data processing approach on the provided level1.fsf template and customized it for our purposes. Spatial smoothing was applied with a full-width at half maximum (FWHM) of 4 mm, and a high-pass filter cutoff of 90 s was used to remove low-frequency noise, as determined by design efficiency estimates calculated within FEAT. Motion correction was performed using MCFLIRT, ensuring precise alignment of images. Registration steps were excluded from the Level 1 analysis because the HCP preprocessing pipelines had already aligned the data to the MNI152 template. The final output consisted of fully filtered 4D fMRI data, which was used for subsequent analyses.

### Pairwise maximum entropy model (PMEM)

The Pairwise Maximum Entropy Model (PMEM) (Watanabe et al. 2013) is a minimalist framework widely applied in neuroscience to investigate the emergence of large-scale brain activation patterns through pairwise interactions between regions of interest (ROIs). In this study, ROIs were defined using spherical masks with a 12 mm diameter, centered on coordinates derived from activation likelihood estimation meta-analyses of the DMN (9 ROIs) and task-related activations for the WMN (12 ROIs) (Laird et al., 2009; Moser et al., 2018). For each ROI, voxel time series were averaged and Z-normalized for subsequent analysis. Based on previous study, a broad range of thresholds can be selected to binarize fMRI signals to get accurate fitting (Watanabe et al. 2013). We select a threshold of 0.6 SD to classify the state of each region as either activated (+1) or deactivated (−1). At any given time  $t$ , the state of brain region  $i$  was represented by the binarized variable  $s_i(t)$ , and the overall system state was described by an  $N$ -dimensional vector  $\vec{s}(t) = [s_1(t), s_2(t), \dots, s_N(t)]$ , where  $N$  is the number of brain regions (see Fig. 2a for an illustration of this step).

The PMEM framework models the statistical features of brain activity by fitting the mean activation ( $\langle s_i \rangle$ ) of each region and the pairwise covariance ( $\langle s_i s_j \rangle$ ) between regions  $i$  and  $j$ . Model parameters  $\theta$  include the external field ( $h_i$ ) representing brain activity level and effective connectivity ( $J_{ij}$ ), resulting in a total of  $M = N + N(N - 1)/2$  parameters, and they can be represented as a  $M$ -dimensional vector  $\vec{\theta}$ . The probability of observing a specific system state  $\vec{s}$ , given parameter  $\vec{\theta}$ , is described by:

$$P(\vec{s}; \vec{\theta}) = \frac{1}{Z} \exp \left[ - \sum_{i=1}^N h_i s_i - \sum_{i < j} J_{ij} s_i s_j \right],$$

where  $Z$  is a normalization constant. The effective connectivities ( $J_{ij}$ ) are thought to reflect underlying structural connectivity and nonlinear dynamics between brain regions, as supported by prior studies (Watanabe et al., 2013; Ashourvan et al., 2021; Jeong et al., 2021).

### Fitting Method

To estimate the external field parameters ( $h_i$ ) and interaction parameters ( $J_{ij}$ ), we initialized  $J_{ij}$  values as Gaussian-distributed variables with a mean of 0 and variance of 1, while initially setting  $h_i$  values to zero. Parameter fitting was performed iteratively using an update rule that minimizes the difference between model and empirical data (Tang et al. 2008):

$$h_i^{\text{new}} = h_i^{\text{old}} - \alpha (\langle s_i \rangle^{\text{model}} - \langle s_i \rangle),$$

$$J_{ij}^{\text{new}} = J_{ij}^{\text{old}} - \alpha(\langle s_i s_j \rangle^{\text{model}} - \langle s_i s_j \rangle),$$

where  $\alpha$  is the learning rate, set to 0.0001. The terms  $\langle s_i \rangle^{\text{model}}$  and  $\langle s_i s_j \rangle^{\text{model}}$  represent the mean and covariances calculated from Monte Carlo simulations of the model based on the parameters from the previous iteration. Superscripts "new" and "old" denote the current and previous parameter values, respectively.

In the Monte Carlo simulations, state transitions of individual brain regions ( $s_i$ , switching between +1 and -1) were governed by the Metropolis criterion. If a proposed new state ( $\vec{s}_{\text{after}}$ ) had a higher probability than the current state ( $\vec{s}_{\text{before}}$ ), it was accepted. For cases where the new state had a lower probability, acceptance was determined probabilistically, with the transition probability ( $P_{\text{MC}}$ ) calculated as:

$$P_{\text{MC}} = \min\left(1, \frac{P(\vec{s}_{\text{after}})}{P(\vec{s}_{\text{before}})}\right) = \min(1, \exp[-\beta(\varepsilon(\vec{s}_{\text{after}}) - \varepsilon(\vec{s}_{\text{before}}))]),$$

where  $\varepsilon(\vec{s}) = \sum_{i=1}^N h_i s_i + \sum_{i<j} J_{ij} s_i s_j$  represents the energy of the system, and  $\beta$  controls the model's activity level and influences fitting efficiency. In our simulations,  $\beta$  was set to 2.

To assess the model's performance, we compared the functional connectivity (FC) simulated by the model with the empirical FC derived from the BOLD signals. FC was calculated using Pearson's correlation coefficients between brain regions  $i$  and  $j$ :

$$\text{FC}(i, j) = \mathbf{E}[s_i s_j] - \mathbf{E}[s_i] \mathbf{E}[s_j],$$

where  $\mathbf{E}[\cdot]$  denotes the expected value of a random variable. This approach ensures robust validation of the model's accuracy in capturing the observed FC patterns.

### Individual- and Group-Level Fitting

For individual-level fitting, we applied the updating rules to the fMRI time series of each participant, iteratively refining the model parameters. The fitting process for a participant was terminated once the similarity between the simulated functional connectivity (FC) and the empirical FC reached a uniform convergence threshold of 0.99. Participants whose fitting process did not converge to this threshold within 1000 iterations were excluded from further analysis. Figure S1a illustrates the overall fitting process across all participants.

To evaluate the predictive accuracy of the group model, we implemented a 10-fold cross-validation approach. The dataset was randomly divided into 10 folds, with one fold used as the training set to fit the group model and the remaining nine folds used as test sets to assess predictability. This process was repeated with shuffled participant orders to generate 10 independent realizations of the 10-fold division. Within each realization, the time series of corresponding brain regions from all individuals in the training set were concatenated and used to fit the group model. Fitting was terminated when it reached an accuracy threshold of 0.98. We slightly lowered the threshold for the group model to ensure convergence of the algorithm for each realization. The results of the fitting process across the 10 realizations are summarized in Figure S1b. The model fitting steps are illustrated in Figure 2b. Parameters of individuals are distributed around the group parameters in the  $M$ -D parameter space and treated as individual differences (see Fig. 1).

### Fisher Information Matrix (FIM)

After obtaining the group model parameters through the fitting process described above, we calculated the Fisher Information Matrix (FIM) to analyze how parameter deviations from the group model affect

the system's state distribution. For a group model with parameter  $\vec{\theta}_0$  and a model with slightly deviated parameter ( $\vec{\theta} = \vec{\theta}_0 + \delta\vec{\theta}$ ), their state the probability distributions are  $P(\vec{s}; \vec{\theta}_0)$  and  $P(\vec{s}; \vec{\theta})$ , respectively. The FIM is fundamentally connected to local changes in probability distributions through its relationship with the Kullback-Leibler (KL) divergence, which is defined as

$$D_{KL}(P(\vec{s}; \vec{\theta}) || P(\vec{s}; \vec{\theta}_0)) = \int p(\vec{s}; \vec{\theta}) \log \frac{P(\vec{s}; \vec{\theta})}{P(\vec{s}; \vec{\theta}_0)} d\vec{s}.$$

With Taylor expansion, the KL divergence can be approximated as:

$$D_{KL}(P(\vec{s}; \vec{\theta}_0 + \delta\vec{\theta}) || P(\vec{s}; \vec{\theta}_0)) \approx D_0 + G\delta\vec{\theta} + \frac{1}{2} \delta\vec{\theta}^T F \delta\vec{\theta} \approx \frac{1}{2} \sum_{l,m} \delta\theta_l F_{l,m} \delta\theta_m,$$

where constant  $D_0$  and the gradient  $G$  will vanish at the optimal group model parameters. Here, matrix  $F$  is known as the observed FIM, and it is the Hessian of the KL divergence with respect to the model parameters,

$$F_{l,m} = \frac{\partial^2(D_{KL})}{\partial\theta_l \partial\theta_m},$$

where  $\theta_l$  is the  $l$ -th dimension of  $\vec{\theta}$ , i.e., the  $l$ -th parameter among the total  $M$  parameters, and  $F_{l,m}$  is the  $(l, m)$ -th entry of the FIM.  $F$  measures how sensitive the system's state distribution is to differences in parameters compared to the group model.

Following the setups of the PMEM (Panas et al., 2015), in our calculations, the FIM entries were computed as:

$$F_{l,m}(\vec{\theta}) = \langle X_l X_m \rangle^{\text{model}} - \langle X_l \rangle^{\text{model}} \langle X_m \rangle^{\text{model}},$$

where  $X_l = s_i$  for parameters  $h_i$ ,  $X_m = s_j s_k$  for couplings  $J_{jk}$ , and  $\langle \cdot \rangle^{\text{model}}$  denotes the average calculated from the Monte Carlo simulations of the model with group parameters. To ensure robustness, we simulated the well-fitted group model 100 times and averaged the resulting FIMs for further analysis.

To study sloppiness property, we conducted the eigendecomposition of the FIM:

$$F = \sum_{k=1}^M \lambda_k v_k v_k^T,$$

yielding eigenvalues ( $\lambda_k$ ) and eigenvectors ( $\vec{v}_k$ ), where larger eigenvalues reflect dimensions in which deviations from the group model parameters have a more pronounced effect on the system's state distribution. Each eigenvector ( $\vec{v}_k$ ) represents a specific weighted profile of variation of the parameters and larger values of the vector components denote stronger sensitivity of a parameter ( $h_i$  or  $J_{ij}$ ) on systems dynamics along the direction of this eigenvector, as illustrated in Figure 2e.

### Effect of Parameter Deviations on Dynamics States

We assessed how deviations from the group model parameters influenced system dynamics using the eigendecomposition of the FIM. Based on the equations above, for a deviation  $\delta\theta$  from the group model, the corresponding KL divergence can be approximated as:

$$D_{KL} \left( P(\vec{s}; \vec{\theta}_0 + \delta\vec{\theta}) \parallel P(\vec{s}; \vec{\theta}_0) \right) \approx \sum_p (w_p(\delta\theta))^2,$$

where  $w_p(\delta\vec{\theta}) = \sqrt{\lambda_p} \vec{v}_p^T \delta\vec{\theta}$  quantifies the impact of parameter deviations along the eigenvector  $\vec{v}_p$ , scaled by its associated eigenvalue  $\lambda_p$ .

By treating individual differences as deviations from the group model, we calculated the contributions of each individual ( $q$ ) to dynamics along the first and second stiffest eigenvectors  $\vec{v}_1$ , as follows:

$$\delta W_1 = \sqrt{\lambda_1} (\vec{\theta}_q - \vec{\theta}_g) \cdot \vec{v}_1, \quad \delta W_2 = \sqrt{\lambda_2} (\vec{\theta}_q - \vec{\theta}_g) \cdot \vec{v}_2,$$

where  $\vec{\theta}_g$  represents the group model parameters. The relative contribution of parameter project on the first eigenvector ( $\vec{v}_1$ ) to the total dynamic differences ( $\delta W_1 + \delta W_2$ ) can be calculated as:

$$\alpha = \frac{\sqrt{\lambda_1}}{\sqrt{\lambda_1} + \sqrt{\lambda_2}}$$

This theoretical estimation was compared to the empirical results of  $\alpha$  in the combined stiff direction  $\vec{v}_{\text{tot}} = \alpha \vec{v}_1 + (1 - \alpha) \vec{v}_2$  for the prediction of individual performance in the WM tasks.

## Supplement

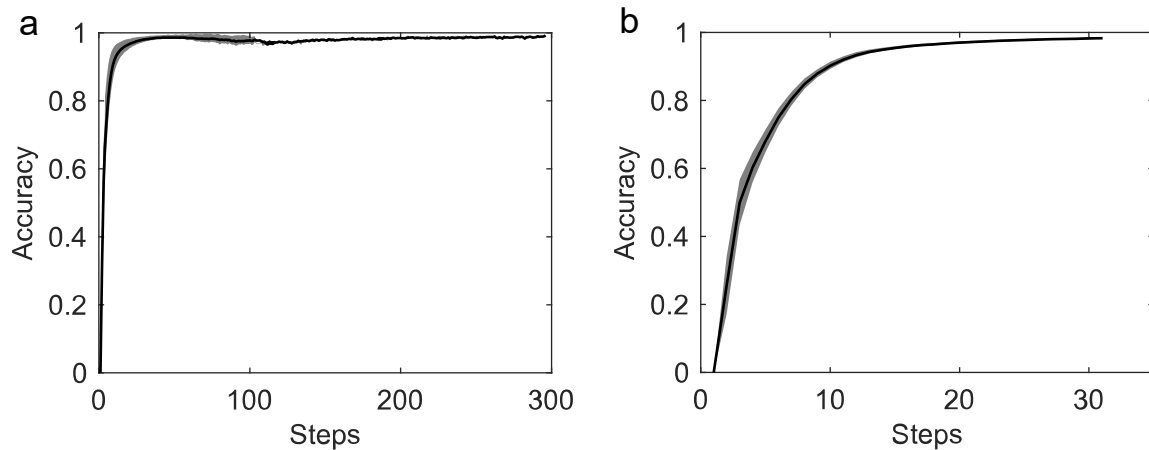


**Figure S1 | Similarity (measured as Pearson's correlation coefficient) between empirical functional connectivity and simulated functional connectivity of the model of individuals (a) and groups (b) during fitting.** (a) Each individual fitting stops when it reaches the accuracy threshold of 0.99 after at most 1000 iterations or else the participant is discarded. Shaded area shows the standard deviation across different participants. (b) Each realization of 10-fold training set of the group model stops fitting when it reaches the accuracy threshold of 0.98. All realizations reached this threshold. Shaded area shows the standard deviation for different realizations of 10 folds.

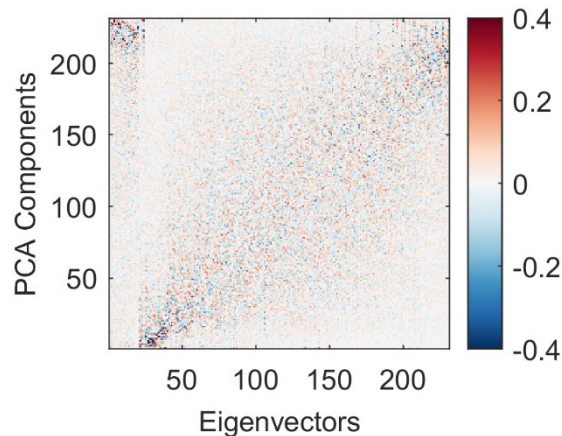


**Figure S2 | Pairwise similarity between PCA components of individual parameters and sensitivity eigenvectors of FIM of group model.** PCA, conducted across participants, captures parameter variance across individuals. The y- and x-axis represent the ranks of PCA components (ranked on loadings) and eigenvectors (ranked on eigenvalues), respectively.

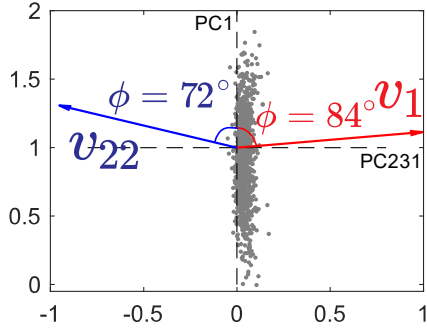


**Figure S3 | Geometric relationship between PCA components and eigenvectors of FIM.** Each gray dot is an individual projection of parameters on the subspace of PC1 and PC231. The surface of eigenvectors ( $v_1$  and  $v_{22}$ ) and the surface of PCs (PC1 and PC231) are not coplanar. Here we measure the angle between PC1 and  $v_1$  and  $v_{22}$ .

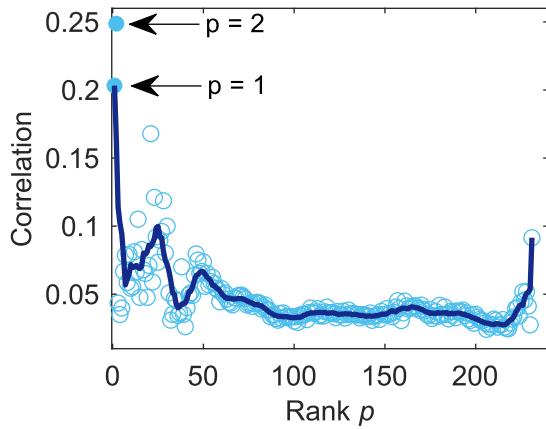


**Figure S4 | Averaged correlation between the predicted  $\eta_p$  and working memory task accuracy of the test sets.** Same as the calculations in Figure 6, the group model was fitted using the training set to derive the stiff directions, which were then used to project individual parameter variations from each test set, yielding predicted  $\eta_p$ . Pearson's correlation was calculated between these predictions and participants' WM performance accuracy. The solid line indicates the moving average (window size 10), and filled circles denote significant correlations ( $p < 10^{-6}$ ).

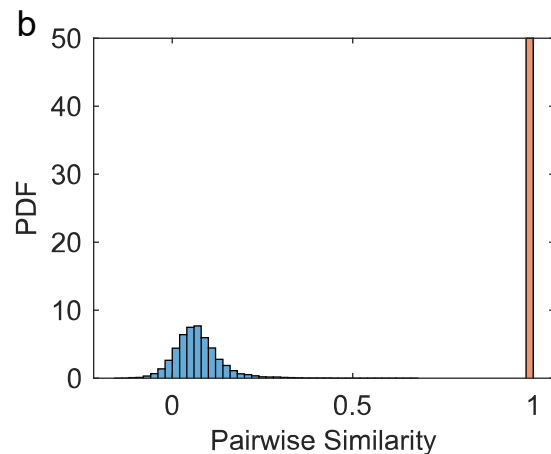
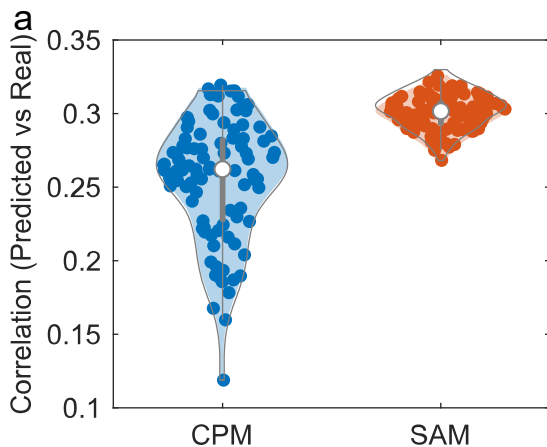


**Figure S5 | Comparison between Connectome Prediction Method (CPM) and the Stiff-Sloppy Analysis Method (SAM).** (a) Correlations between predicted working memory task accuracy and real working memory task accuracy. Each dot is a realization of 10-fold cross validation. In each realization, CPM will select several significant connections from training set as features, and our stiff-sloppy analysis method will generate stiff direction from training set. (b) Consistency of features (selected connections) in CPM and our stiff direction. For each realization, we choose the optimal  $\alpha = 0.48$  the same as Figure 6b. Probability Density Function (PDF) describes the relative likelihood of a continuous random variable taking on a specific value. The area under the PDF curve over an interval gives the probability of the variable falling within that range.

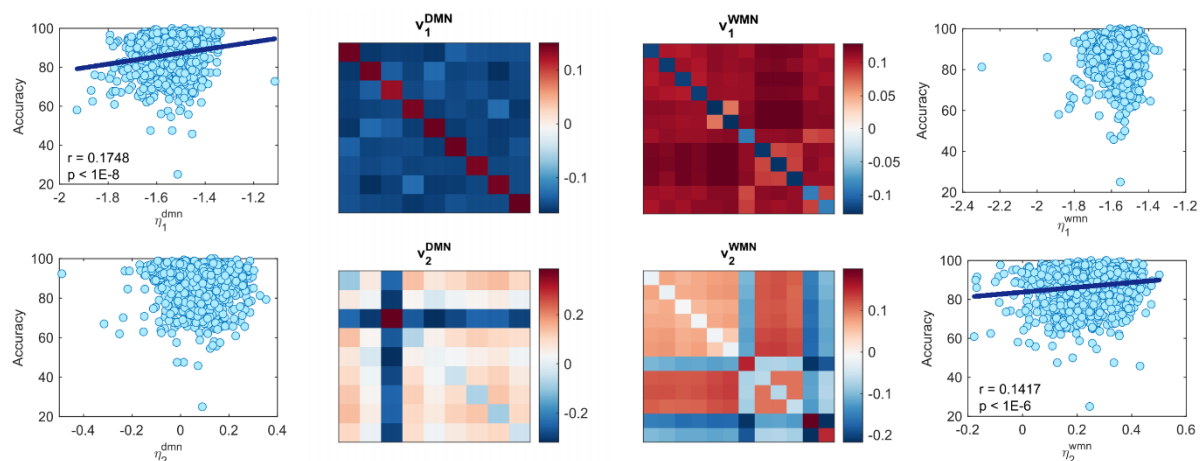


**Figure S6 | DMN-only vs. WMN-only Models.** To highlight the importance of integrating and segregating different functional networks in explaining individual working memory task performance, we fitted models exclusively on either DMN or WMN for all participants and conducted sloppiness analyses. The figures illustrate corresponding eigenvectors and Pearson's correlation between task performance in the working memory task and  $\eta_1$  and  $\eta_2$  when using only the two functional subnetworks separately.

## References

- Anticevic, A., M. W. Cole, J. D. Murray, P. R. Corlett, X. J. Wang and J. H. Krystal (2012). "The role of default network deactivation in cognition and disease." *Trends Cogn Sci* **16**(12): 584-592.
- Baker, J. T., A. J. Holmes, G. A. Masters, B. T. Yeo, F. Krienen, R. L. Buckner and D. Ongur (2014). "Disruption of cortical association networks in schizophrenia and psychotic bipolar disorder." *JAMA Psychiatry* **71**(2): 109-118.
- Barch, D. M., G. C. Burgess, M. P. Harms, S. E. Petersen, B. L. Schlaggar, M. Corbetta, M. F. Glasser, S. Curtiss, S. Dixit, C. Feldt, D. Nolan, E. Bryant, T. Hartley, O. Footer, J. M. Bjork, R. Poldrack, S. Smith, H. Johansen-Berg, A. Z. Snyder, D. C. Van Essen and W. U.-M. Consortium (2013). "Function in the human connectome: task-fMRI and individual differences in behavior." *Neuroimage* **80**: 169-189.
- Baumeister, R. F. (2007). *Encyclopedia of social psychology*, Sage.
- Bouchard, T. J., Jr. and M. McGue (2003). "Genetic and environmental influences on human psychological differences." *J Neurobiol* **54**(1): 4-45.

Brookes, M. J., J. R. Wood, C. M. Stevenson, J. M. Zumer, T. P. White, P. F. Liddle and P. G. Morris (2011). "Changes in brain network activity during working memory tasks: a magnetoencephalography study." Neuroimage **55**(4): 1804-1815.

Bullmore, E. and O. Sporns (2009). "Complex brain networks: graph theoretical analysis of structural and functional systems." Nat Rev Neurosci **10**(3): 186-198.

Cole, M. W., J. R. Reynolds, J. D. Power, G. Repovs, A. Anticevic and T. S. Braver (2013). "Multi-task connectivity reveals flexible hubs for adaptive task control." Nat Neurosci **16**(9): 1348-1355.

Drysdale, A. T., L. Grosenick, J. Downar, K. Dunlop, F. Mansouri, Y. Meng, R. N. Fetcho, B. Zebley, D. J. Oathes, A. Etkin, A. F. Schatzberg, K. Sudheimer, J. Keller, H. S. Mayberg, F. M. Gunning, G. S. Alexopoulos, M. D. Fox, A. Pascual-Leone, H. U. Voss, B. J. Casey, M. J. Dubin and C. Liston (2017). "Resting-state connectivity biomarkers define neurophysiological subtypes of depression." Nat Med **23**(1): 28-38.

Faisal, A. A., L. P. Selen and D. M. Wolpert (2008). "Noise in the nervous system." Nat Rev Neurosci **9**(4): 292-303.

Finn, E. S., X. Shen, D. Scheinost, M. D. Rosenberg, J. Huang, M. M. Chun, X. Papademetris and R. T. Constable (2015). "Functional connectome fingerprinting: identifying individuals using patterns of brain connectivity." Nat Neurosci **18**(11): 1664-1671.

Fox, M. D., R. L. Buckner, M. P. White, M. D. Greicius and A. Pascual-Leone (2012). "Efficacy of transcranial magnetic stimulation targets for depression is related to intrinsic functional connectivity with the subgenual cingulate." Biol Psychiatry **72**(7): 595-603.

Fox, M. D., A. Z. Snyder, J. L. Vincent, M. Corbetta, D. C. Van Essen and M. E. Raichle (2005). "The human brain is intrinsically organized into dynamic, anticorrelated functional networks." Proc Natl Acad Sci U S A **102**(27): 9673-9678.

Gratton, C., T. O. Laumann, A. N. Nielsen, D. J. Greene, E. M. Gordon, A. W. Gilmore, S. M. Nelson, R. S. Coalson, A. Z. Snyder and B. L. Schlaggar (2018). "Functional brain networks are dominated by stable group and individual factors, not cognitive or daily variation." Neuron **98**(2): 439-452. e435.

Gutenkunst, R. N., J. J. Waterfall, F. P. Casey, K. S. Brown, C. R. Myers and J. P. Sethna (2007). "Universally sloppy parameter sensitivities in systems biology models." PLoS Comput Biol **3**(10): 1871-1878.

Hampson, M., N. Driesen, J. K. Roth, J. C. Gore and R. T. Constable (2010). "Functional connectivity between task-positive and task-negative brain areas and its relation to working memory performance." Magn Reson Imaging **28**(8): 1051-1057.

Honey, C. J., J. P. Thivierge and O. Sporns (2010). "Can structure predict function in the human brain?" Neuroimage **52**(3): 766-776.

MacDonald, S. W., S. C. Li and L. Backman (2009). "Neural underpinnings of within-person variability in cognitive functioning." Psychol Aging **24**(4): 792-808.

Medaglia, J. D., M. E. Lynall and D. S. Bassett (2015). "Cognitive network neuroscience." J Cogn Neurosci **27**(8): 1471-1491.

Moser, D. A., G. E. Doucet, A. Ing, D. Dima, G. Schumann, R. M. Bilder and S. Frangou (2018). "An integrated brain-behavior model for working memory." Mol Psychiatry **23**(10): 1974-1980.

Panas, D., H. Amin, A. Maccione, O. Muthmann, M. van Rossum, L. Berdondini and M. H. Hennig (2015). "Sloppiness in spontaneously active neuronal networks." J Neurosci **35**(22): 8480-8492.

Ponce-Alvarez, A., G. Mochol, A. Hermoso-Mendizabal, J. de la Rocha and G. Deco (2020). "Cortical state transitions and stimulus response evolve along stiff and sloppy parameter dimensions, respectively." Elife **9**.

Ponce-Alvarez, A., L. Uhrig, N. Deco, C. M. Signorelli, M. L. Kringelbach, B. Jarraya and G. Deco (2022). "Macroscopic Quantities of Collective Brain Activity during Wakefulness and Anesthesia." *Cereb Cortex* **32**(2): 298-311.

Raichle, M. E. (2015). "The brain's default mode network." *Annu Rev Neurosci* **38**: 433-447.

Rosenberg, M. D., E. S. Finn, D. Scheinost, X. Papademetris, X. Shen, R. T. Constable and M. M. Chun (2016). "A neuromarker of sustained attention from whole-brain functional connectivity." *Nat Neurosci* **19**(1): 165-171.

Shen, X., E. S. Finn, D. Scheinost, M. D. Rosenberg, M. M. Chun, X. Papademetris and R. T. Constable (2017). "Using connectome-based predictive modeling to predict individual behavior from brain connectivity." *Nat Protoc* **12**(3): 506-518.

Shine, J. M., P. G. Bissett, P. T. Bell, O. Koyejo, J. H. Balsters, K. J. Gorgolewski, C. A. Moodie and R. A. Poldrack (2016). "The Dynamics of Functional Brain Networks: Integrated Network States during Cognitive Task Performance." *Neuron* **92**(2): 544-554.

Smith, S. M., T. E. Nichols, D. Vidaurre, A. M. Winkler, T. E. J. Behrens, M. F. Glasser, K. Ugurbil, D. M. Barch, D. C. Van Essen and K. L. Miller (2015). "A positive-negative mode of population covariation links brain connectivity, demographics and behavior." *Nature Neuroscience* **18**(11): 1565-1567.

Tang, A., D. Jackson, J. Hobbs, W. Chen, J. L. Smith, H. Patel, A. Prieto, D. Petrusca, M. I. Grivich, A. Sher, P. Hottowy, W. Dabrowski, A. M. Litke and J. M. Beggs (2008). "A maximum entropy model applied to spatial and temporal correlations from cortical networks in vitro." *J Neurosci* **28**(2): 505-518.

Thompson, P. M., T. D. Cannon, K. L. Narr, T. van Erp, V. P. Poutanen, M. Huttunen, J. Lonnqvist, C. G. Standertskjold-Nordenstam, J. Kaprio, M. Khaledy, R. Dail, C. I. Zoumalan and A. W. Toga (2001). "Genetic influences on brain structure." *Nat Neurosci* **4**(12): 1253-1258.

Wang, R., M. Liu, X. Cheng, Y. Wu, A. Hildebrandt and C. Zhou (2021). "Segregation, integration, and balance of large-scale resting brain networks configure different cognitive abilities." *Proc Natl Acad Sci U S A* **118**(23).

Watanabe, T., S. Hirose, H. Wada, Y. Imai, T. Machida, I. Shirouzu, S. Konishi, Y. Miyashita and N. Masuda (2013). "A pairwise maximum entropy model accurately describes resting-state human brain networks." *Nat Commun* **4**: 1370.

Woolrich, M. W., S. Jbabdi, B. Patenaude, M. Chappell, S. Makni, T. Behrens, C. Beckmann, M. Jenkinson and S. M. Smith (2009). "Bayesian analysis of neuroimaging data in FSL." *Neuroimage* **45**(1 Suppl): S173-186.